Research Square

Preprints are preliminary reports that have not undergone peer review.
They should not be considered conclusive, used to inform clinical practice,
or referenced by the media as validated information.

Metal-organic framework derived cobalt oxides modified by N-doped carbon nanotubes as bifunctional electrocatalyst for Zn-air battery

Yan Ding
Jilin Business and Technology College
Li Fang
No.2 Middle School, Xinjiang Production and Construction Corps 12th Division
Xinxin Xu
xuxx@mail.neu.edu.cn

Northeastern University

Research Article

Keywords: Electrocatalysis, ORR and OER, Zn-air battery, Cobalt oxides, MOF

Posted Date: November 25th, 2026

DOI: https://doi.org/10.21203/rs.3.rs-11395367/v1

License: This work is licensed under a Creative Commons Attribution 4.0 International License.
Read Full License

Additional Declarations: No competing interests reported.

Metal-organic framework derived cobalt oxides modified by N-doped carbon nanotubes as bifunctional electrocatalyst for Zn-air battery

Yan Ding,[a] Li Fang,[b] and Xinxin Xu[c]*

[a] School of Grain engineering and Nutritional Science, Jilin Business and Technology College, Changchun 130507, China

[b] No.2 Middle School, Xinjiang Production and Construction Corps 12th Division, Urumqi, Xinjiang Uygur Autonomous Region, 830000, China

[c] Department of Chemistry, College of Science, Northeastern University, Shenyang 110819, Liaoning, China

*Author to whom correspondence should be addressed.

Tel: +86-024-83684533, Fax: +86-024-83684533.

E-mail: xuxx@mail.neu.edu.cn (Prof. X. X. Xu)

Abstract

Because of high power density, specific capacitance and low cost, Zn-air battery has received great attention. For Zn-air battery, oxygen reduction reaction (ORR) and oxygen evolution reaction (OER) are involved in discharging and charging processes. But both ORR and OER suffer from sluggish kinetics, which makes the development of efficient ORR and OER electrocatalysts become an urgent task. Herein, with a Co-based Metal-Organic Framework (MOF) as precursor, bifunctional electrocatalyst is synthesized. In this electrocatalyst, CoO and Co_3O_4 particles dope in N-doped carbon nanotubes (NCNTs) derived from dicyandiamide (DCDA). In alkaline electrolyte, its half-wave potential ($E_{1/2}$) and limiting current density (J_d) achieve 0.843 V and 5.59 $mA \cdot cm^{-2}$. In OER, the overpotential and Tafel slope are 350 mV and 60.2 $mV \cdot dec^{-1}$. Based on the promising ORR and OER activities, Zn-air battery is constructed. Its open-circuit voltage and peak power density reach 1.46 V and 128.2 $mW \cdot cm^{-2}$. The specific capacity and energy density of Zn-air battery are 850.63 $mAh \cdot g^{-1}$ and 1020.72 $Wh \cdot kg^{-1}$ at 5 $mA \cdot cm^{-2}$. The battery also shows perfect rating capacity and promising long-time charge/discharge performance. This work develops an excellent Co-based bifunctional electrocatalyst as cathode material in Zn-air battery.

Keywords: Electrocatalysis; ORR and OER; Zn-air battery; Cobalt oxides; MOF

Introduction

With the increasingly severe energy crisis and environmental pollution, it is urgent to develop energy conversion devices such as fuel cells and metal batteries.[1] The application of metal-air batteries provides a more convenient and eco-friendly way in making the use of renewable energy.[2] As a member in the family of metal-air batteries, Zn-air battery has received great attention due to its high power density, low cost and compact size.[3] During discharging process, ORR occurs, while in charging process, OER is involved.[4] However, the sluggish ORR and OER impede the energy utilization and transfer rate of Zn-air battery severely.[5] To resolve this problem, the development of bifunctional electrocatalysts with excellent efficiency and stability becomes a feasible method.[6]

Traditional noble metal (Pt, Ir and Ru) based electrocatalysts have been widely concerned due to their attractive ORR and OER activities.[7] Nonetheless, the expensive cost, scarcity and low stability limit their practical application greatly.[8] To address above problems, substantial scientists have made great effort and found non-metal materials, especially carbon based materials can be regarded as promising alternatives for noble metal based electrocatalysts.[9] Carbon nanotube (CNT) possesses the characteristics of abundant resources, low price and extraordinary bifunctional OER/ORR activities, which has attracted vast investigations.[10-16] Its “tubes” character enhances the specific area and provides more active sites during electrocatalysis.[17-20] Furthermore, CNTs crisscross each other, which can speed up the electron transfer and improve electrocatalytic activities.[21-23] In addition, N doping nitrogen in CNTs can induce charge distribution in CNTs. NCNTs can also provide more active points in ORR and OER.[24-26]

Transition metal based electrocatalysts have triggered extensive research interest

because of their rich active sites and perfect electrocatalytic activity.[27-30] Meanwhile, it has been confirmed that transition metal oxides have high ORR and OER activities.[31-35] Their activities can be further improved after encapsulated in NCNTs. In this aspect, cobalt oxides (such as Co_3O_4 and CoO) have been considered as the ideal alternatives to noble metal based electrocatalysts for their easy-making and high electrocatalytic activities.[36-38] To ensure the efficiency of Zn-air battery, a four-electron transfer process is expected. It has been demonstrated that cobalt oxides both shows four-electron character in ORR.[39-43] Furthermore, the introduction of cobalt oxides in NCNTs matrix can improve the conductivity and electron transfer speed. This is benefit for further enhancement of electrocatalytic activities.

Based on above mentioned points, with $[Co(PDCA)(H_2O)_2]_n$ (**CoMOF**, PDCA = 3,5-Pyridinedicarboxylic acid), a Co-MOF as precursor, bifunctional electrocatalyst (**CoO/Co_3O_4@NCNTs(A)**) was synthesized. In its structure, CoO/Co_3O_4 particles with the size about 30 to 40 nm distribute homogeneously in bamboo-shaped NCNTs derived from DCDA (Scheme 1). It shows perfect ORR activity. In 0.1 M KOH, its $E_{1/2}$ achieves 0.843 V. The OER activity of **CoO/Co_3O_4@NCNTs(A)** is promising. Its η_{10} value is merely 350 mV with Tafel slope 60.2 $mV \cdot dec^{-1}$. Zn-air battery is constructed with **CoO/Co_3O_4@NCNTs(A)** as cathode material. Its peak density reaches 128.2 $mW \cdot cm^{-2}$. At 5 $mA \cdot cm^{-2}$, its specific capacity and energy density are 850.63 $mAh \cdot g^{-1}$ and 1020.72 $Wh \cdot kg^{-1}$. Zn-air battery also possesses attractive rating capacity and perfect long-time charge/discharge performance.

Experimental section

Synthesis of CoMOF

$Co(NO_3)_2 \cdot 6H_2O$ (0.582 g, 2 mmol) and PDCA (0.334 g, 2 mmol) were dissolved in H_2O (16 ml). The pH value of obtained solution was adjusted to 5.0 by 1 M KOH.

After stirred for 30 min, the mixture was transferred into Teflon lined autoclave (20 mL) and heated at 180 °C for 96 h. After cooling to room temperature, the red crystals were washed and dried in a vacuum oven at 80 °C for 12 h.

Synthesis of CoO/Co_3O_4@NCNTs(A)

DCDA (2.5 g, on gas inlet side) and **CoMOF** (0.15 g, on gas outlet side) were dispersed on both sides of porcelain boat. After heated at 750 °C in tube furnace under N_2 protection for 2 h, black **CoO/Co_3O_4@NCNTs(A)** was obtained. The products were washed with water and dried at 80 °C for 12 h.

Synthesis of CoO/Co_3O_4@NCNTs(B)

DCDA (2.5 g, on gas inlet side) and ZIF-67 (0.15 g, on gas outlet side) were dispersed on both sides of porcelain boat. After heated at 750 °C in tube furnace under N_2 protection for 2 h, black **CoO/Co_3O_4@NCNTs(B)** was obtained. The products were washed with water and dried at 80 °C for 12 h. ZIF-67 was synthesized based on previous works.

Results and discussion

Structure of CoMOF

The detail structure of **CoMOF** was analyzed with single X-ray diffraction technique. In the fundamental unit, there exists one crystallographically independent Co^{2+} ion. It connects with two carboxylic oxygen atoms and one nitrogen from PDCA ligands with Co(1)-N(1) = 2.196 Å and Co(1)-O(2) = 2.147 Å. As for the bond angles, N(1)-Co(1)-O(2) = 140.14° and O(2)-Co(1)-O(2) = 79.72°. The other two coordination sites of Co^{2+} ion is occupied by two water molecules with Co(1)-O(3) = 2.086 Å. This results the triangular pyramid coordination mode of Co(1) (Fig. S1). For PDCA ligand, it connects with three Co^{2+} ions by two carboxylic oxygen atoms and one nitrogen atom (Fig. S2). With this manner, adjacent Co^{2+} ions are connected and generate

two-dimensional layer structure (Fig. 1a). Furthermore, there exist intensive hydrogen bonds between neighboring layers with O(2)-H(2) = 2.029 Å, O(2)-H(2)-O(3) = 140.8° and O(1)-H(1) = 1.898 Å, O(1)-H(1)-O(3) = 155.29°. These hydrogen bonds connect neighboring layer together and form three-dimensional supramolecular network of **CoMOF** (Fig. 1b). The hydrogen bond lengths and angles are consistence with above reported examples.

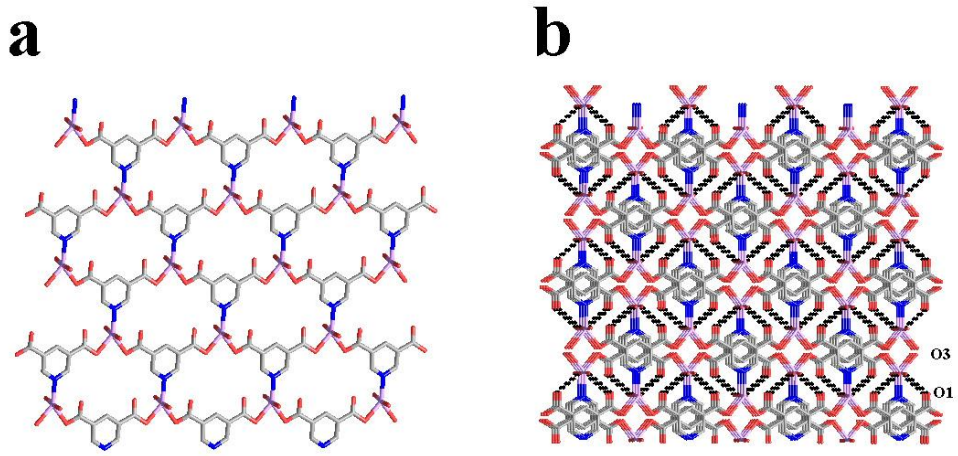

Fig. 1. (a) two-dimensional layer structure and (b) three-dimensional supramolecular network of **CoMOF**.

Structure and morphology of CoO/Co_3O_4@NCNTs(A)

The X-ray diffraction (XRD) measurement was taken to investigate the structure of the calcinated product of **CoMOF**. The peaks match with Co_3O_4 (42-1467) and CoO (43-1004) perfectly (Fig. S3). This demonstrates **CoMOF** converts to Co_3O_4 and CoO after calcinations. As for ZIF-67, the calcinated product shows similar XRD patterns with **CoMOF**, which also suggests CoO and Co_3O_4 generate after calcination (Fig. S4). The structure of calcinated product was further studied with Raman spectrum. Two distinctive peaks at 1351 and 1588 cm^{-1} appear (Fig. S5).[44] They can be ascribed to D and G bands of carbon material, which refer to carbon atoms in disorder and graphite phase respectively. In general, high I_D/I_G indicates a lot of defects exist. In

contrast, low I_D/I_G reveals graphite arrangement of carbon atoms. Here, the value is 1.03, which illustrates a large number of defects exist in calcinated product. This is benefit for further improvement of ORR and OER activities.

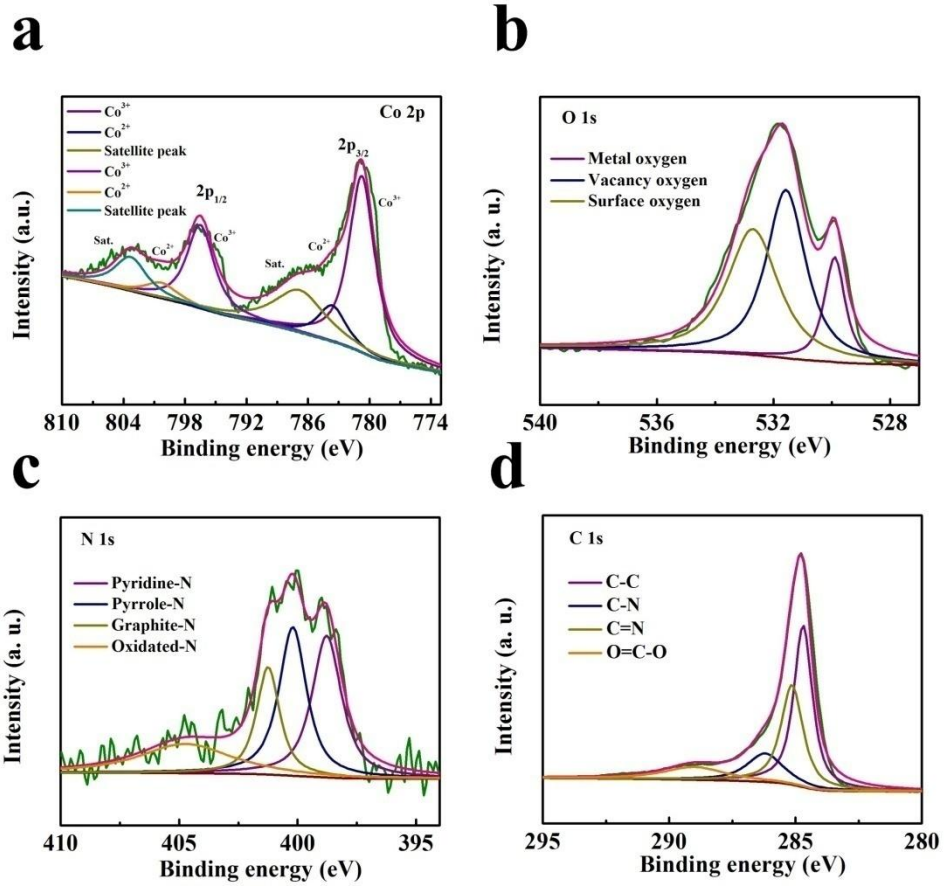

Fig. 2. high resolution (a) Co 2p; (b) O 1s; (c) N 1s; (d) C 1s XPS spectrum of **CoO/Co_3O_4@NCNTs(A)**.

X-ray Photoelectron Spectroscopy (XPS) analysis was conducted to further evaluate the chemical states and composition of **CoO/Co_3O_4@NCNTs(A)**. In survey spectrum, the peaks belonging to Co 2p, O 1s, N 1s and C 1s are detected (Fig. S6). More detail information can be obtained from high resolution spectrum. In high resolution Co 2p spectrum, the first doublet peaks at 780.7 and 796.5 eV can be ascribed to Co $2p_{3/2}$ and Co $2p_{1/2}$ in Co^{3+} state (Fig. 2a).[45] Another pair of peaks at 783.6 and 800.3 eV corresponds with Co $2p_{3/2}$ and Co $2p_{1/2}$ in Co^{2+} state. The remained peaks at 786.9 and 803.3 eV root from satellite peaks of Co. As for high

resolution O 1s spectrum, the peaks at 530.1, 531.6 and 532.8 eV can be attributed to lattice oxygen, oxygen vacancy and oxygen absorbed on surface (Fig. 2b).[46] In high resolution N 1s spectrum, there also exist three peaks, which can be attributed to pyridinic N (398.7 eV), pyrrolic-N (400.2 eV), graphitic-N (401.3 eV) and N in oxidized state (404.5 eV) (Fig. 2c).[47] Graphitic-N can enhance conductivity, which further improves ORR and OER activities. In high resolution C 1s spectrum, four peaks emerge at 284.7, 285.1, 286.2 and 289.1 eV (Fig. 2d). They originate from C=C, C-N, C=N and C=O, respectively.[48]

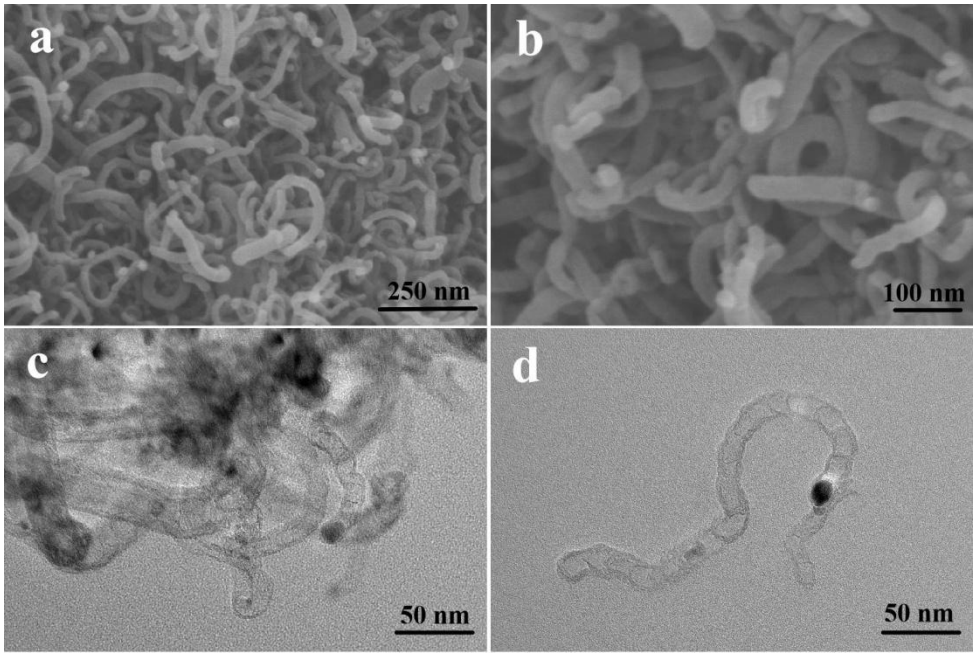

Fig. 3. (a) and (b) SEM images of **CoO/Co_3O_4@NCNTs(A)**; (c) TEM and (d) high resolution TEM images of **CoO/Co_3O_4@NCNTs(A)**.

To evaluate the morphology of **CoO/Co_3O_4@NCNTs(A)**, scanning electron microscope (SEM) were employed. In SEM image, uniform NCNTs with diameter about 60 to 80 nm can be observed clearly, which root from DCDA (Fig. 3a and 3b). NCNTs shows smooth surface. The NCNTs can provide rich active points in electrocatalytic process, which further improves ORR and OER activities. More detail morphological information can be provided by transmission electron microscopy

(TEM). In TEM image, NCNTs can also be found, which possesses similar dimension with SEM image (Fig. 3c). Furthermore, small particles with the size about 30 to 50 nm are also observed, which distributes homogenously in NCNTs (Fig. 3d). In high resolution transmission electron microscopy (HRTEM) image, the lattice fringe about 0.25 and 0.26 nm are found in above mentioned small particles (Fig. S7). They correspond to (311) and (311) planes of Co_3O_4 and CoO perfectly.

ORR activity study

To study the ORR activity of **CoO/Co_3O_4@NCNTs(A)**, linear sweep voltammetry (LSV) experiment are conducted in KOH (0.1M) electrolyte saturated by O_2. For **CoO/Co_3O_4@NCNTs(A)**, its $E_{1/2}$ achieves 0.843 V (Fig. 4a). This value is higher obviously than **CoO/Co_3O_4@NCNTs(B)** (0.835 V) and Pt/C (0.840 V). The J_d value of **CoO/Co_3O_4@NCNTs(A)** reaches 5.59 $mA \cdot cm^{-2}$, which is also higher greatly than **CoO/Co_3O_4@NCNTs(B)** (4.89 $mA \cdot cm^{-2}$) and Pt/C (4.68 $mA \cdot cm^{-2}$). All these facts demonstrate the superior electrocatalytic ORR activity of **CoO/Co_3O_4@NCNTs(A)** over **CoO/Co_3O_4@NCNTs(B)**. The ORR activity of **CoO/Co_3O_4@NCNTs(A)** was also evaluated by cyclic voltammetry (CV) technique. It shows more positive oxygen reduction peak (0.821 V) than Pt/C (0.812 V) (Fig. 4b). This further illustrates higher electrocatalytic activity of **CoO/Co_3O_4@NCNTs(A)** than Pt/C in ORR.

To evaluate the potential of an electrocatalyst in practical application, the stability is a crucial factor. Here, the stability of **CoO/Co_3O_4@NCNTs(A)** was evaluated by comparing the $E_{1/2}$ value before and after 5000 cycles LSV test. At first, the $E_{1/2}$ of **CoO/Co_3O_4@NCNTs(A)** is 0.843 V. After 5000 cycles LSV test, its $E_{1/2}$ value still keeps at 0.839 V (Fig. 4c). In this process, the J_d value also keeps unchanged. All these facts illustrate the excellent stability of **CoO/Co_3O_4@NCNTs(A)** in real application. The stability of **CoO/Co_3O_4@NCNTs(A)** can also be judged by

chronoamperometric curves at constant potential. After ORR experiment lasted for 12 h, the current density still retains at 96.1% (Fig. 4d). As for Pt/C, only 80.1% activity keeps after 12 h experiment. All these facts demonstrate the promising stability of **CoO/Co$_3$O$_4$@NCNTs(A)** in ORR.

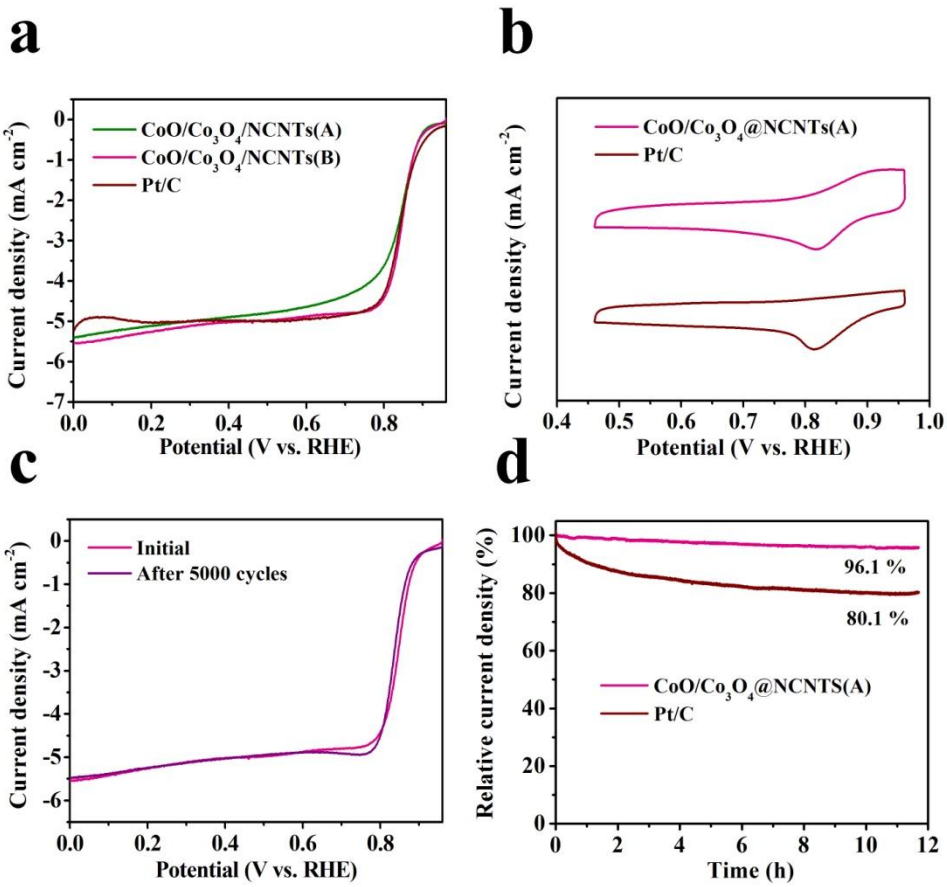

Fig. 4. (a) RDE voltammograms of different electrocatalysts at 1600 rpm; (b) CV curves of different electrocatalysts; (c) LSV curves before and after 5000 cycles ORR test of **CoO/Co$_3$O$_4$@NCNTs(A)**; (d) the chronoamperometric curves of different electrocatalysts in ORR.

To study the electron transfer number in ORR, rotating ring-disk electrode (RRDE) technique was used. **CoO/Co$_3$O$_4$@NCNTs(A)** shows higher disk current density than **CoO/Co$_3$O$_4$@NCNTs(B)** and Pt/C in 0.1 M KOH (Fig. 5a). The H_2O_2 selectivity of **CoO/Co$_3$O$_4$@NCNTs(A)** ranges from 9.27 to 10.77%, with electron transfer number increasing from 3.81 to 3.86 (Fig. 5b and 5c). As for **CoO/Co$_3$O$_4$@NCNTs(B)**, the

H_2O_2 selectivity fluctuate between 13.6 and 15.7%. Its electron transfer number ranges from 3.66 to 3.70. The electron transfer number of **CoO/Co$_3$O$_4$@NCNTs(A)** and **CoO/Co$_3$O$_4$@NCNTs(B)** are further determined by rotating disk electrode (RDE) technique. Their LSV curves were recorded with rotation rates increasing from 400 to 2500 rpm. With the increasing of rotating speed, the current density also enhances (Fig. 5d and S8). Simulated from Koutecky-Levich (K-L) equation at 0.4, 0.5, 0.6 and 0.7 V (vs. RHE), the electron transfer numbers of **CoO/Co$_3$O$_4$@NCNTs(A)** are 3.99, 3.97, 3.96 and 3.95 (Fig. 5e, 5f and S9).[49] As for **CoO/Co$_3$O$_4$@NCNTs(B)**, the electron transfer numbers are 3.95, 3.92, 3.91 and 3.88. These results imply they both show 4e-character in ORR.

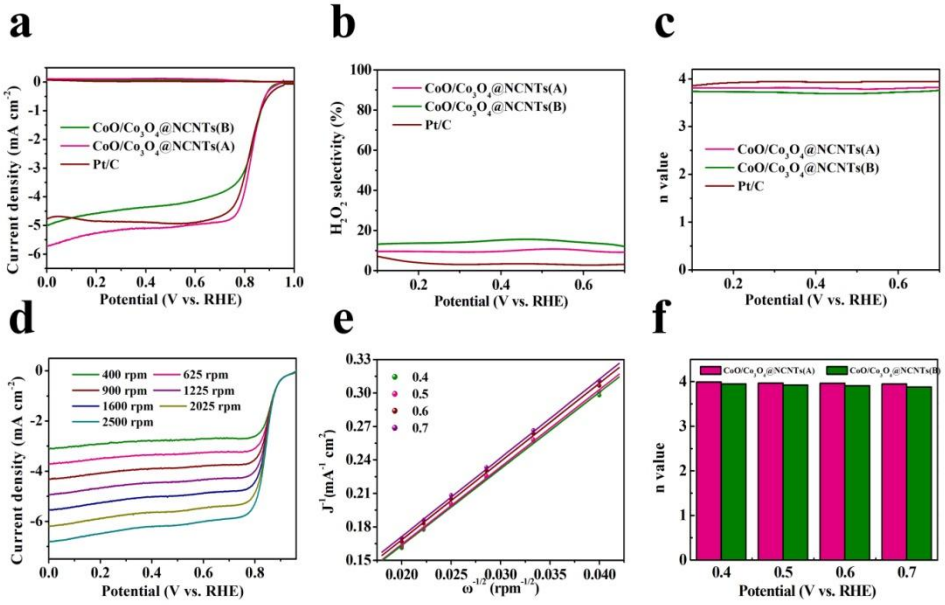

Fig. 5. (a) RRDE voltammograms of different electrocatalysts at 1600 rpm; (b) H_2O_2 selectivity and (c) n value of different electrocatalysts; (d) LSV curves of **CoO/Co$_3$O$_4$@NCNTs(A)** under different scanning rates; (e) K-L equation simulation and (f) n values of **CoO/Co$_3$O$_4$@NCNTs(A)** under different potentials.

OER activity study

The OER activities of **CoO/Co$_3$O$_4$@NCNTs(A)** and **CoO/Co$_3$O$_4$@NCNTs(B)**

were both studied with three-electrode system. For **CoO/Co$_3$O$_4$@NCNTs(A)**, the η_{10} value is 350 mV (Fig. 6a). The η_{10} value of **CoO/Co$_3$O$_4$@NCNTs(B)** achieves 420 mV. Tafel slope further claims that **CoO/Co$_3$O$_4$@NCNTs(A)** shows a lower Tafel slope (60.2 mV·dec^{-1}) than **CoO/Co$_3$O$_4$@NCNTs(B)** (68.8 mV·dec^{-1}), which results in faster reaction kinetics and enhanced OER performance (Fig. 6b). To explore difference OER activity between these electrocatalysts, electrochemical impedance spectroscopy (EIS) was conducted. Nyquist diagram shows **CoO/Co$_3$O$_4$@NCNTs(A)** exhibits smaller semicircle diameter than **CoO/Co$_3$O$_4$@NCNTs(B)** (Fig. 6c). This demonstrates **CoO/Co$_3$O$_4$@NCNTs(A)** shows lower charge transfer resistance than **CoO/Co$_3$O$_4$@NCNTs(B)**, which improves electron movement and enhances OER.

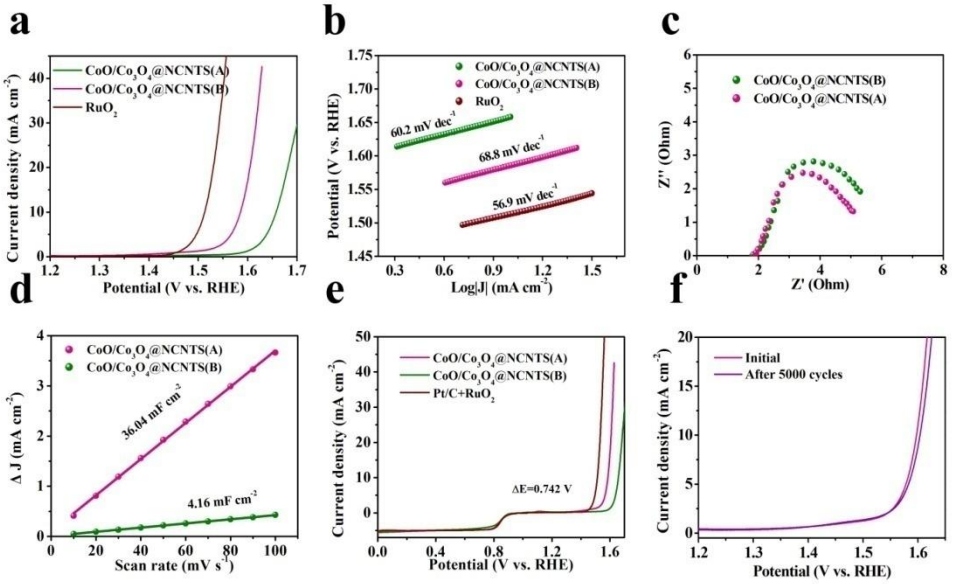

Fig. 6. (a) LSV curves of different electrocatalysts in OER; (b) Tafel plots of different electrocatalysts; (c) Nyquist plots and (d) C_{dl} values of different electrocatalysts; (e) ΔE values for different electrocatalysts; (f) LSV curves of **CoO/Co$_3$O$_4$@NCNTs(A)** in OER, before and after 5000 cycles tests.

Electrochemical double-layer capacitance (C_{dl}) was calculated based on CV curves at different scan rates from 20 to 100 mV·s^{-1} (Fig. S10 and S11). The C_{dl} value of **CoO/Co$_3$O$_4$@NCNTs(A)** achieves as high as 36.04 mF·cm^{-2}, which is higher than

CoO/Co$_3$O$_4$@NCNTs(B) (4.16 mF·cm^{-2}) (Fig. 6d). Since C_{dl} value is positively correlated with electrochemical active surface area (ECSA) in electrocatalysis, the results illustrate **CoO/Co$_3$O$_4$@NCNTs(A)** can provide more active points than **CoO/Co$_3$O$_4$@NCNTs(B)**.[50] To study the stability of **CoO/Co$_3$O$_4$@NCNTs(A)**, LSV curves at the first and 5000 cycles are recorded and compared (Fig. 6e). The η_{10} value exhibits a subtle change from 350 mV to 368 mV, confirming it is suitable for practical OER in Zn-air battery. The potential gap (ΔE) between $E_{1/2}$ in ORR and η_{10} in OER is a crucial parameter to investigate the overall ORR and OER performance of electrocatalyst.[51] For **CoO/Co$_3$O$_4$@NCNTs(A)**, the ΔE is merely 0.715 V (Fig. 6f). This indicates it is an extraordinary bifunctional electrocatalyst, which is suitable to be applied as a cathode material for Zn-air battery.

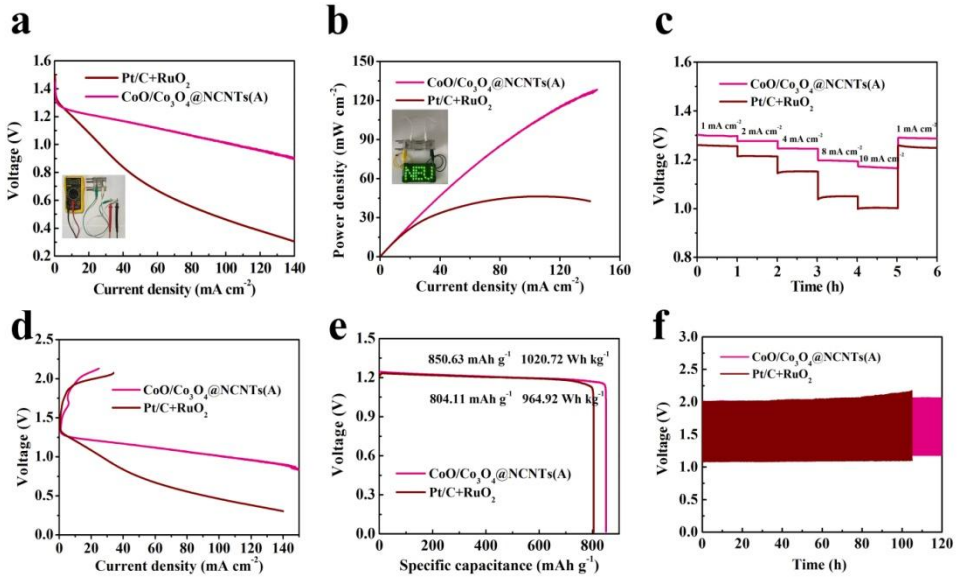

Fig. 7. (a) polar curves of Zn-air battery, inset, photograph of one Zn-air battery; (b) power density curves of Zn-air battery; inset, photograph of LED lights powered by two Zn-air batteries linked in series; (c) galvanostatic discharge curve of at 1, 2, 4, 8 and 10 mA·cm^{-2}; (d) charge/discharge polar curves of Zn-air battery; (e) galvanostatic discharge curves at 1, 5 and 10 mA·cm^{-2}; (f) recycled charge/discharge test at 1 mA·cm^{-2} for 120 h.

Charge-discharge performance of Zn-air battery

Considering the perfect ORR and OER activities, rechargeable Zn-air battery was assembled with **CoO/Co_3O_4@NCNTS(A)** as cathode material. In this battery, polished zinc plate acts as anode and 6.0 M KOH containing 0.2 M $Zn(OAc)_2$ employs as electrolyte. The Zn-air battery possesses a high open-circuit voltage of 1.46 V (Fig. 7a and 7a inset). This is higher than Zn-air battery composed by Pt/C+RuO_2. At 1.0 V, this Zn-air battery can provide high current density of 112.1 $mA \cdot cm^{-2}$. It can deliver an ideal peak power density of 128.2 $mW \cdot cm^{-2}$, which is higher significantly than 46.3 $mW \cdot cm^{-2}$ of Pt/C+RuO_2 (Fig. 7b). With two Zn-air batteries connected with series mode, green light-emitting diodes (LED, theoretical voltage about 2.2 V) can be lit up for more than 12 h (Fig. 7b, inset). Galvanostatic technique was chosen to study the rate capacity of this Zn-air battery. At 1, 2, 4, 8 and 10 $mA \cdot cm^{-2}$, the voltage plateau locate at 1.30, 1.28, 1.24, 1.19 and 1.17 V (Fig. 7c). After discharging for 5 h, the current density goes back to 1 $mA \cdot cm^{-2}$, the voltage still keeps at 1.29 V. This confirms perfect rate capacity of this Zn-air battery.

The specific capacitance of Zn-air battery were studied at 5 $mA \cdot cm^{-2}$ with galvanostatic technique. At 5 $mA \cdot cm^{-2}$, the specific capacitance achieve as high as 850.63 $mAh \cdot g^{-1}$ based on the mass of Zn consumed (Fig. 7d). For Zn-air battery composed by Pt/C+RuO_2, the specific capacitance is merely 804.11 $mAh \cdot g^{-1}$ at 5 $mA \cdot cm^{-2}$. The energy density of Zn-air battery is 1020.72 $Wh \cdot kg^{-1}$, which is higher than Zn-air battery composed by Pt/C+RuO_2 (964.92 $Wh \cdot kg^{-1}$). Furthermore, the discharge and charge polarization curves depicts the Zn-air battery possesses low charge-discharge voltage gap. At 25 $mA \cdot cm^{-2}$, the charge-discharge voltage gap is merely 0.91 V, which is adjacent to the battery built by Pt/C+RuO_2 (1.08 V) (Fig. 7e). Low charge-discharge voltage gap confirms perfect recharge ability and high power

conversion efficiency of this Zn-air battery. In order to evaluate the stability of Zn-air battery composed by **CoO/Co_3O_4@NCNTs(A)**, long-term charge-discharge test were conducted at 1 $mA \cdot cm^{-2}$. With galvanostatic technology, each charge-discharge cycle last for 1 h (0.5 h for charge and 0.5 h for discharge). In 120 h charge-discharge test, the charge and discharge voltages keep at 2.06 and 1.16 V throughout (Fig. 7f). For Zn-air battery built by Pt/C+RuO_2, its charge and discharge voltages can only keep stable before 60 h.

Conclusions

In summary, bifunctional ORR/OER electrocatalyst, **CoO/Co_3O_4@NCNTs(A)**, is synthesized successfully with a Co-based MOF as precursor. In the structure, CoO/Co_3O_4 particles distribute homogenously in DCDA derived NCNTs. In ORR, **CoO/Co_3O_4@NCNTs(A)** exhibits high $E_{1/2}$ and J_d in alkaline electrolyte. As for OER, **CoO/Co_3O_4@NCNTs(A)** possesses low η_{10} value and Tafel slope. Based on the promising ORR and OER activities of **CoO/Co_3O_4@NCNTs(A)**, Zn-air battery is constructed. The Zn-air battery shows perfect charge and discharge performance with high specific capacity, energy density and power density. Furthermore, its rating capacity and long-time charge-discharge performance is also attractive. We anticipate this work finds an efficient method to improve the ORR and OER activities for Co based bifunctional electrocatalyst in Zn-air battery.

Supplementary information: **the online version contains supplementary material available at:**

Author contribution:

Yan Ding: investigation, writing original draft, data treatment and formal analysis; **Li Fang**: data treatment and formal analysis; **XinxinXu**: review, supervision, funding acquisition and resources.

Funding: this work was supported by National Natural Science Foundation of China (22171039), Science and Technology Development Project Foundation of Jilin Business and Technology College (ZD2026[001]) and Natural Science Foundation of Jilin Science and Technology Department (20260102124JC).

Ethical approval: this research did not involve human or animal samples.

Conflict of interest: the authors declare no competing interests.

Data availability statement: the authors confirm that the data supporting the findings of this study are available on request.

References

[1] Y. Gao, D. Zheng, Q. Li, W. Xiao, T. Ma, Y. Fu, Z. Wu, L. Wang, 3D Co_3O_4-RuO_2 Hollow Spheres with Abundant Interfaces as Advanced Trifunctional Electrocatalyst for Water-Splitting and Flexible Zn-Air Battery, Adv. Funct. Mater. 32(38) (2022) 2203206. https://doi.org/10.1002/adfm.202203206.

[2] H. Li, G. Yan, H. Zhao, P.C. Howlett, X. Wang, J. Fang, Earthworm-Inspired Co/Co_3O_4/CoF_2@NSC Nanofibrous Electrocatalyst with Confined Channels for Enhanced ORR/OER Performance, Adv. Mater. 36(26) (2024) 202311272. https://doi.org/10.1002/adma.202311272.

[3] W. Wu, R. chen, S. Chen, Z. Wang, N. Cheng, Optimizing d-Orbital Electronic Configuration via Metal-Metal Oxide Core-Shell Charge Donation for Boosting Reversible Oxygen Electrocatalysis, Small 19(25) (2023) 202300621. https://doi.org/10.1002/smll.202300621.

[4] Y. Zhang, Z. Zhang, G. Jiang, A.H. Mamaghani, S. Sy, R. Gao, Y. Jiang, Y. Deng, Z. Bai, L. Yang, A. Yu, Z. Chen, Three-dimensionally ordered mesoporous Co_3O_4

decorated with Mg as bifunctional oxygen electrocatalysts for high-performance zinc-air batteries, Nano Energy 100 (2022) 107425. https://doi.org/10.1016/j.nanoen.2022.107425.

[5] Q. Huang, X. Zhong, Q. Zhang, X. Wu, M. Jiao, B. Chen, J. Sheng, G. Zhou, Co_3O_4/Mn_3O_4 hybrid catalysts with heterointerfaces as bifunctional catalysts for Zn-air batteries, Journal of Energy Chemistry 68 (2022) 679-687. https://doi.org/10.1016/j.jechem.2021.12.032.

[6] B. He, Y. Deng, H. Wang, R. Wang, J. Jin, Y. Gong, L. Zhao, Metal organic framework derived perovskite/spinel heterojunction as efficient bifunctional oxygen electrocatalyst for rechargeable and flexible Zn-air batteries, J. Colloid Interface Sci. 625 (2022) 502-511. https://doi.org/10.1016/j.jcis.2022.06.048.

[7] X. Zhao, Q. Han, J. Li, X. Du, G. Liu, Y. Wang, L. Wu, Z. Chen, Ordered macroporous design of sacrificial Co/VN nano-heterojunction as bifunctional oxygen electrocatalyst for rechargeable zinc-air batteries, Chem. Eng. J. 433 (2022) 133509. https://doi.org/10.1016/j.cej.2021.133509.

[8] Y. Chen, S. Qiao, Y. Tang, Y. Du, D. Zhang, W. Wang, H. Zhang, X. Sun, C. Liu, Double-Faced Atomic-Level Engineering of Hollow Carbon Nanofibers as Free-Standing Bifunctional Oxygen Electrocatalysts for Flexible Zn–Air Battery, ACS Nano 16(9) (2022) 15273-15285. https://doi.org/10.1021/acsnano.2c06700.

[9] J. Jo, J.M. Yoo, D.H. Mok, H.Y. Jang, J. Kim, W. Ko, K. Yeom, M.S. Bootharaju, S. Back, Y.-E. Sung, T. Hyeon, Facet-Defined Strain-Free Spinel Oxide for Oxygen Reduction, Nano Lett. 22(9) (2022) 3636-3644. https://doi.org/10.1021/acs.nanolett.2c00238.

[10] X. He, J. Xu, F. Yin, J. Li, R. Ma, B. Chen, Low temperature route to Co, N, O tri-decorated carbon nanotubes: Moderate defects toward boosted bifunctional oxygen

electrocatalysis and Zn-air batteries, Appl. Surf. Sci. 616 (2023) 156450. https://doi.org/10.1016/j.apsusc.2023.156450.

[11] M. Wu, X. Yang, X. Cui, N. Chen, L. Du, M. Cherif, F.-K. Chiang, Y. Wen, A. Hassanpour, F. Vidal, S. Omanovic, Y. Yang, S. Sun, G. Zhang, Engineering Fe-N_4 Electronic Structure with Adjacent Co-N2C2 and Co Nanoclusters on Carbon Nanotubes for Efficient Oxygen Electrocatalysis, Nano-Micro Lett. 15(1) (2023). https://doi.org/10.1007/s40820-023-01195-2.

[12] M. Wang, S. Zhang, J. Teng, S. Zhao, Z. Li, M. Wu, Combination of Mn-Mo Oxide Nanoparticles on Carbon Nanotubes through Nitrogen Doping to Catalyze Oxygen Reduction, Molecules 28(14) (2023) 5544. https://doi.org/10.3390/molecules28145544.

[13] E. Mysliu, M. Scavini, S. Santangelo, S. Patanè, N. Ditaranto, P. Bassani, M. Longhi, Enhanced ORR activity of S- and N-modified non-noble metal-doped carbons with bamboo-like C nanotubes grafted onto their surface, Electrochim. Acta 464 (2023) 142946. https://doi.org/10.1016/j.electacta.2023.142946.

[14] C. Dong, Z.-Q. Wang, C. Yang, X. Hu, P. Wang, X.-Q. Gong, L. Lin, X.-y. Li, Sequential electrocatalysis by single molybdenum atoms/clusters doped on carbon nanotubes for removing organic contaminants from wastewater, Appl. Catal. B 338 (2023) 123060. https://doi.org/10.1016/j.apcatb.2023.123060.

[15] E.Y. Choi, D.E. Kim, S.Y. Lee, C.B. Park, C.K. Kim, Cobalt nanoparticles-encapsulated holey nitrogen-doped carbon nanotubes for stable and efficient oxygen reduction and evolution reactions in rechargeable Zn-air batteries, Appl. Catal. B 325 (2023) 122386. https://doi.org/10.1016/j.apcatb.2023.122386.

[16] Y. Nie, X. Xu, X. Wang, M. Liu, T. Gao, B. Liu, L. Li, X. Meng, P. Gu, J. Zou, CoNi Alloys Encapsulated in N-Doped Carbon Nanotubes for Stabilizing Oxygen

Electrocatalysis in Zinc-Air Battery, Nanomaterials 13(11) (2023) 1788. https://doi.org/10.3390/nano13111788.

[17] Z. Zhao, Y. Xiong, S. Yu, T. Fang, K. Yi, B. Yang, Y. Zhang, X. Yang, X. Liu, X. Jia, Single-atom Zn with nitrogen defects on biomimetic 3D carbon nanotubes for bifunctional oxygen electrocatalysis, J. Colloid Interface Sci. 650 (2023) 934-942. https://doi.org/10.1016/j.jcis.2023.06.182.

[18] Y. Chen, J. Niu, Y. Pei, H. Song, Y. Fan, S. Lu, B. Liu, Methanol-reduced Pd nanoparticles anchored on B,N-CDs@CNT hybrid for oxygen reduction reaction, Int. J. Hydrogen Energy 48(13) (2023) 5116-5125. https://doi.org/10.1016/j.ijhydene.2022.11.054.

[19] Y. Xu, R. Xie, Q. Li, J. Feng, H. Luo, Q. Ye, Z. Guo, Y. Cao, M. Palma, G. Chai, M.M. Titirici, C.R. Jones, Pyridine Functionalized Carbon Nanotubes: Unveiling the Role of External Pyridinic Nitrogen Sites for Oxygen Reduction Reaction, Small 19(45) (2023) 2302795. https://doi.org/10.1002/smll.202302795.

[20] X. Meng, J. Xie, J. Liu, B. Liu, R. Wang, P. Gu, F. Ma, X. Wang, J. Zou, Co_3C-stabilized-CoFe heterostructure wrapped by bamboo-like N-doped carbon nanotubes for highly-efficient oxygen electrocatalysis, Chem. Eng. J. 459 (2023) 141591. https://doi.org/10.1016/j.cej.2023.141591.

[21] D.-H. Wu, H. Huang, M. Ul Haq, L. Zhang, J.-J. Feng, A.-J. Wang, Lignin-derived iron carbide/Mn, N, S-codoped carbon nanotubes as a high-efficiency catalyst for synergistically enhanced oxygen reduction reaction and rechargeable zinc-air battery, J. Colloid Interface Sci. 647 (2023) 1-11. https://doi.org/10.1016/j.jcis.2023.05.111.

[22] H. Hu, P. Zhang, B.-B. Xiao, J.-L. Mi, Substrate Strain Engineering of Single-Atomic Sn-N4 Sites Embedded in Various Carbon Matrixes for Bifunctional

Oxygen Electrocatalysis, ACS Appl. Mater. Interfaces 15(19) (2023) 23170-23184. https://doi.org/10.1021/acsami.3c02232.

[23] Y. Chen, Y. Wu, L. Li, Y. Liao, S. Luo, H. Xu, Y. Wu, Y. Qing, Hierarchical wood cells impose well-textured carbon nanotubes with cobalt single atoms: Bioinspired construction and application in zinc–air battery, Chem. Eng. J. 475 (2023) 145993. https://doi.org/10.1016/j.cej.2023.145993.

[24] S. Ajmal, A. Kumar, G. Yasin, M.M. Alam, M. Selvaraj, M. Tabish, M.A. Mushtaq, R.K. Gupta, W. Zhao, A microwave-assisted decoration of carbon nanotubes with Fe_3O_4 nanoparticles for efficient electrocatalytic oxygen reduction reaction, J. Alloys Compd. 943 (2023) 169067. https://doi.org/10.1016/j.jallcom.2023.169067.

[25] Q. Guo, S. Ma, Q.-L. Wu, Z.-Z. Liu, Z.-Q. Yao, S. Li, J.-P. Zhao, F.-C. Liu, Gradual introduction of multiple active sites in quest of high activity metal-free oxygen reduction catalysts and exploring the synergistic effect, Inorg. Chem. Front. 10(13) (2023) 3867-3873. https://doi.org/10.1039/d3qi00586k.

[26] A. Situ, T. Zhao, Y. Huang, P. Li, L. Yang, Z. Zhang, Z. Wang, Y. Ou, X. Guan, J. Wen, J. Zhang, Y. Zhan, X. Tang, Dual-MOFs-Derived Fe and Mn Species Anchored on Bamboo-like Carbon Nanotubes for Efficient Oxygen Reduction as Electrocatalysts, Catalysts 13(8) (2023) 1161. https://doi.org/10.3390/catal13081161.

[27] A. Behera, D. Seth, M. Agarwal, M.A. Haider, A.J. Bhattacharyya, Exploring Cu-Doped Co_3O_4 Bifunctional Oxygen Electrocatalysts for Aqueous Zn–Air Batteries, ACS Appl. Mater. Interfaces 16(14) (2024) 17574-17586. https://doi.org/10.1021/acsami.4c00571.

[28] Z. Xia, B. Deng, Y. Wang, Z. Jiang, Z.-J. Jiang, Synergistic co-doping induced high catalytic activities of La/Fe doped Co_3O_4 towards oxygen reduction/evolution reactions for Zn–air batteries, J. Mater. Chem. A 10(44) (2022) 23483-23493.

https://doi.org/10.1039/d2ta06726a.

[29] V. Kepenienė, R. Stagniūnaitė, S. Rafique, J. Vaičiūnienė, V. Jasulaitiene, V. Pakštas, Z. Sukackienė, R. Vilkauskaite, L. Tamašauskaitė-Tamašiūnaitė, E. Norkus, Pd-Supported Co_3O_4/C Catalysts as Promising Electrocatalytic Materials for Oxygen Reduction Reaction, Catalysts 12(8) (2022) 920. https://doi.org/10.3390/catal12080920.

[30] J. Liu, J. Xie, R. Wang, B. Liu, X. Meng, X. Xu, B. Tang, Z. Cai, J. Zou, Interfacial electron modulation of Cu_2O by Co_3O_4 embedded in hollow carbon cube skeleton for boosting oxygen reduction/revolution reactions, Chem. Eng. J. 450 (2022) 137961. https://doi.org/10.1016/j.cej.2022.137961.

[31] J. Zhang, J. Lian, Q. Jiang, G. Wang, Boosting the OER/ORR/HER activity of Ru-doped Ni/Co oxides heterostructure, Chem. Eng. J. 439 (2022) 135634. https://doi.org/10.1016/j.cej.2022.135634.

[32] B. Chutia, S. Patowary, A. Misra, K.N. Rao, P. Bharali, Morphology Effect of Co3O4 Nanooctahedron in Boosting Oxygen Reduction and Oxygen Evolution Reactions, Energy Fuels 36(22) (2022) 13863-13872. https://doi.org/10.1021/acs.energyfuels.2c02672.

[33] T. Hu, W. Zhang, Z. Xia, Y. Zhu, Y. Liu, J. Zhang, L. Li, Growth restriction of Co_3O_4 nanoparticles by α-MnO2 nanorods as air cathode catalyst for rechargeable aluminum-air battery, Int. J. Energy Res. 46(8) (2022) 11174-11184. https://doi.org/10.1002/er.7917.

[34] Z. Liu, Y. Cao, S. Wang, Z. Lu, J. Hu, J. Xie, A. Hao, Nitrogen-doped strategy derived Co_3O_4/carbon nanosheets as high-performance oxygen electrocatalysis for rechargeable zinc-air batteries application, J. Alloys Compd. 965 (2023) 171479. https://doi.org/10.1016/j.jallcom.2023.171479.

[35] H. Tan, X. Liu, M. Wang, H. Huang, P. Huang, Co3O4 Supported on Graphene-like Carbon by One-Step Calcination of Cobalt Phthalocyanine for Efficient Oxygen Reduction Reaction under Alkaline Medium, Nanomaterials 13(7) (2023) 1241. https://doi.org/10.3390/nano13071241.

[36] X. Zhang, Q. Liu, S. Liu, E. Wang, Manganese-doped cobalt spinel oxide as bifunctional oxygen electrocatalyst toward high-stable rechargeable Zn-air battery, Electrochim. Acta 437 (2023) 141477. https://doi.org/10.1016/j.electacta.2022.141477.

[37] J. Milikić, S. Knežević, M. Ognjanović, D. Stanković, L. Rakočević, B. Šljukić, Template-based synthesis of Co_3O_4 and Co_3O_4/SnO_2 bifunctional catalysts with enhanced electrocatalytic properties for reversible oxygen evolution and reduction reaction, Int. J. Hydrogen Energy 48(71) (2023) 27568-27581. https://doi.org/10.1016/j.ijhydene.2023.03.433.

[38] X. Sun, T. Xu, W. Sun, J. Bai, C. Li, Ce-doped ZIF-67 derived Co_3O_4 nanoparticles supported by carbon nanofibers: A synergistic strategy towards bifunctional oxygen electrocatalysis and Zn-Air batteries, J. Alloys Compd. 898 (2022) 162778. https://doi.org/10.1016/j.jallcom.2021.162778.

[39] J.-W. Park, Y.-W. Ju, Evaluation of Bi-Functional Electrochemical Catalytic Activity of Co_3O_4-$CoFe_2O_4$ Composite Spinel Oxide, Energies 16(1) (2022) 173. https://doi.org/10.3390/en16010173.

[40] Y. Zhang, C. Huang, J. Lu, H. Cao, C. Zhang, X.S. Zhao, Ni-modified Co_3O_4 with competing electrochemical performance to noble metal catalysts in both oxygen reduction and oxygen evolution reactions, Appl. Surf. Sci. 651 (2024) 159241. https://doi.org/10.1016/j.apsusc.2023.159241.

[41] C. Huang, Y. Zhang, X. Li, H. Cao, Y. Guo, C. Zhang, Mn-incorporated Co_3O_4

bifunctional electrocatalysts for zinc-air battery application: An experimental and DFT study, Appl. Catal. B 319 (2022) 121909. https://doi.org/10.1016/j.apcatb.2022.121909.

[42] P. Leng, F. Luo, M. Li, S. Ma, X. Long, Z. Yang, Construction of abundant $Co_3O_4/Co(OH)_2$ heterointerfaces as air electrocatalyst for flexible all-solid-state zinc-air batteries, Electrochim. Acta 413 (2022) 140158. https://doi.org/10.1016/j.electacta.2022.140158.

[43] X. Xu, W. Zhang, Y. Li, P. Wang, Y. Zhang, Synthesis of $Co_3O_4@TiO_2$ catalysts for oxygen evolution and oxygen reduction reactions, Microporous and Mesoporous Materials 335 (2022) 111844. https://doi.org/10.1016/j.micromeso.2022.111844.

[44] J. Hernández-Ferrer, M. Gracia-Martín, A.M. Benito, W.K. Maser, E. García-Bordejé, Effect of temperature and presence of minor amount of metal on porous carbon materials derived from ZIF-8 pyrolysis for electrocatalysis, Catal. Today 423 (2023) 113993. https://doi.org/10.1016/j.cattod.2022.12.024.

[45] F. Gui, Q. Jin, D. Xiao, Z. Jin, Y. Zhang, Y. Cao, M. Yang, Q. Tan, C. Zhang, S. Siahrostami, Q. Xiao, High-performance zinc–air batteries enabled by hybridizing atomically dispersed FeN2 with Co3O4 nanoparticles, J. Mater. Chem. A 11(3) (2023) 1312-1323. https://doi.org/10.1039/d2ta08305a.

[46] C.-C. Weng, X.-W. Lv, J.-T. Ren, Y.-S. Wang, W.-W. Tian, L.-J. Gao, H.-Y. Wang, Z.-Y. Yuan, Self-Promoted Electrocatalysts Derived from Surface Reconstruction for Rechargeable Zinc–Air Batteries, ACS Sustainable Chem. Eng. 10(19) (2022) 6456-6465. https://doi.org/10.1021/acssuschemeng.2c01568.

[47] N. Wang, X. Zheng, Y. Buba, H. Wang, X. Wang, Y. Zhao, Electrocatalytic performance of cobalt/nickel nanoparticles encapsulated by N-doped carbon nanotubes toward the oxygen reduction reaction, Appl. Surf. Sci. 615 (2023) 156317.

https://doi.org/10.1016/j.apsusc.2022.156317.

[48] J. Xu, B. Xue, C. Xia, C. Liu, M. Li, R. Xiao, Transforming bio-oil into nitrogen-doped hierarchical porous carbons: Excellent oxygen reduction electrocatalysts for Zn-air batteries, J. Alloys Compd. 947 (2023) 169584. https://doi.org/10.1016/j.jallcom.2023.169584.

[49] Y. Zheng, X. Xu, J. Chen, Q. Wang, Surface O2- regulation on POM electrocatalyst to achieve accurate 2e/4e-ORR control for H_2O_2 production and Zn-air battery assemble, Appl. Catal. B 285 (2021) 119788. https://doi.org/10.1016/j.apcatb.2020.119788.

[50] Y. Bian, R. Wang, X. Xu, J. Chen, Q. Wang, A wheel-like polyoxometalate for haloperoxidase-inspired antibiofouling with H_2O_2in situ provided by electrocatalysis, Inorg. Chem. Front. 11(10) (2024) 3047-3055. https://doi.org/10.1039/d4qi00482e.

[51] X. Cui, Y. Tao, X. Xu, G. Yang, P-doping optimized d-band center position in MoO_2 with enhanced oxygen reduction reaction and oxygen evolution reaction activities for rechargeable Zn-air battery, J. Power Sources 557 (2023) 232519. https://doi.org/10.1016/j.jpowsour.2022.232519.

Metal-organic framework derived cobalt oxides modified by N-doped carbon nanotubes as bifunctional electrocatalyst for Zn-air battery

Yan Ding,[a] Li Fang,[b] and Xinxin Xu[c]*

[a] School of Grain engineering and Nutritional Science, Jilin Business and Technology College, Changchun 130507, China

[b] No.2 Middle School, Xinjiang Production and Construction Corps 12th Division, Urumqi, Xinjiang Uygur Autonomous Region, 830000, China

[c] Department of Chemistry, College of Science, Northeastern University, Shenyang 110819, Liaoning, China

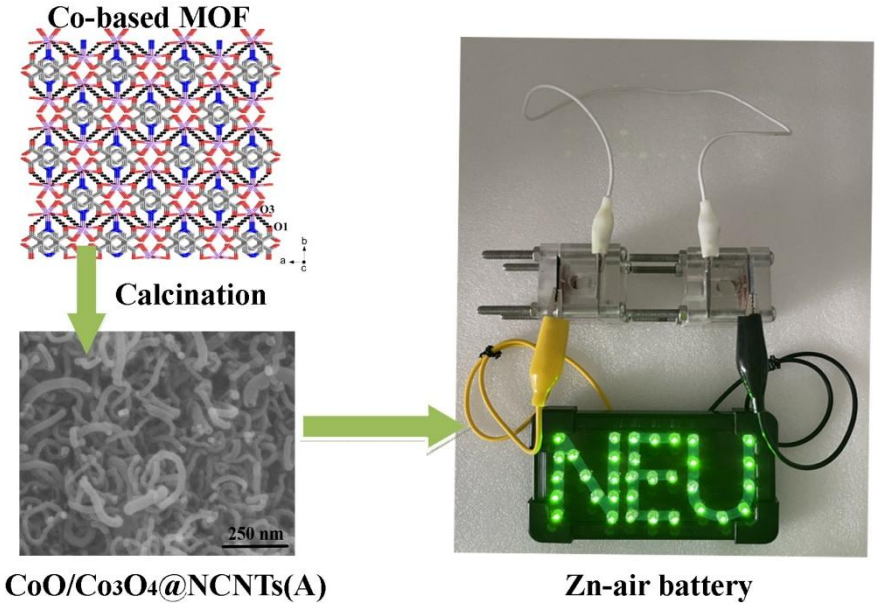

Based on Co-based MOF, bifunctional electrocatalyst was synthesized with perfect ORR and OER activities, which can be used as cathode material in Zn-air battery.

Supplementary Files

This is a list of supplementary files associated with this preprint. Click to download.

- ElectronicSupplementaryMaterial.docx